ELSEVIER

*Computers and Geotechnics*, Vol. 19, No. 3, pp. 245–263, 1996

PII: S0266-352X(96)00002-X 0266-352X/96/$15.00+0.00

# Influence of Viscous Damping in the Dynamic Analysis of an Earth Dam Using Simple Constitutive Models

P. K. Woodward[a] & D. V. Griffiths[b]

[a]Department of Civil & Offshore Engineering, Heriot-Watt University, Edinburgh, U.K.

[b]Geomechanics Research Center, Colorado School of Mines, Golden, CO, U.S.A.

(Received 21 December 1994; revised version received 27 November 1995; accepted 21 December 1995)

## *ABSTRACT*

*The results of dynamic non-linear two-dimensional finite element analyses of the Long Valley Dam in the Mammoth Lake area of California subjected to a real measured earthquake are presented. A simple elastic–perfectly plastic constitutive soil model is used to describe the stress–strain response of the soil and Rayleigh damping (i.e. viscous damping) is applied to account for the lack of hysteretic damping. The effect of the initial stress condition and the Rayleigh damping ratio are discussed, and the results of the analysis are compared to the measured response of the dam and to results presented by previous researchers. Good agreement is obtained in the up/downstream direction, but as experienced by previous researchers, the correct vertical frequency range is not achieved. The limitations of using viscous damping combined with simple constitutive models when studying the dynamic behaviour of real earth dams are shown. Copyright © 1996 Elsevier Science Ltd.*

## INTRODUCTION

The Long Valley Dam [1] consists of a large rolled impervious earthfill core underneath a compacted embankment of more permeable material (Fig. 1). Due to the large clay core the entire dam is essentially saturated, and a two-phase analysis, in which the soil and water are treated separately is not required. The dam is built in a narrow canyon, 240 miles north of the city of Los Angeles close to the Sierra Frontal fault and the Hilton Creek fault

systems. In 1980 a series of earthquakes in the Mammoth Lakes area close to the Long Valley Dam in California were monitored. The dam is instrumented with a multi-channel central-recording accelerograph system with all instruments

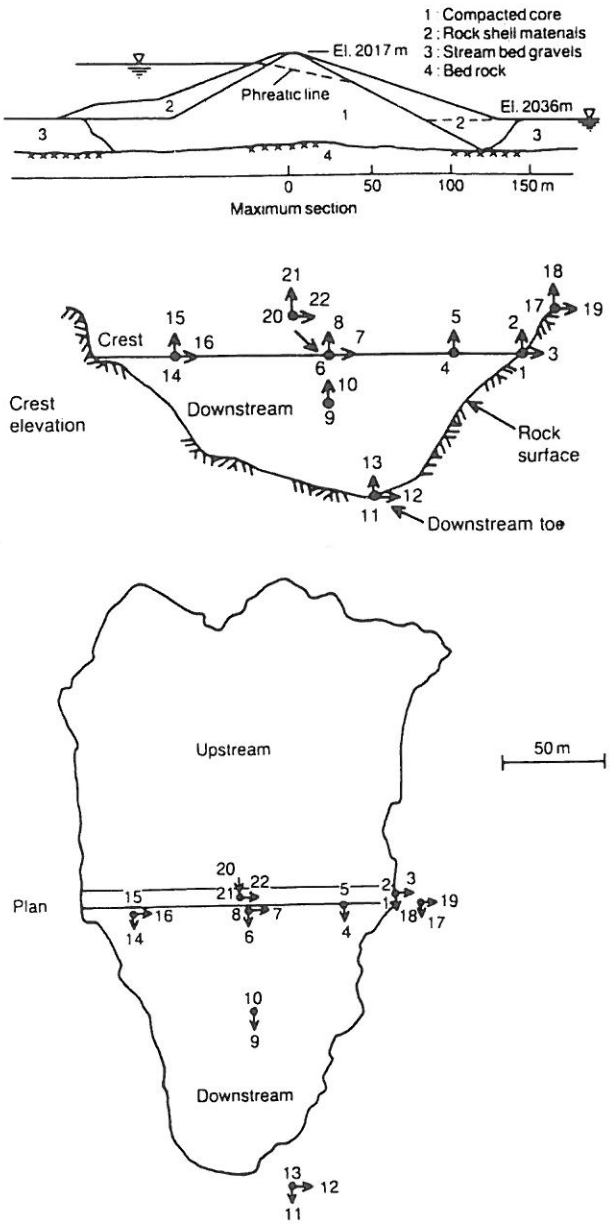


**Fig. 1.** Details of the Long Valley Dam and location of the strong motion instrumentation (Griffiths and Prevost [4]).

tied together. During the series of earthquakes 22 of the accelerographs on or near to the dam triggered [2], providing an extensive array of earthquake acceleration time histories. The largest earthquake experienced by the dam occurred on 27 May 1980 resulting in peak upstream/downstream horizontal and vertical crest accelerations of 0·47 $g$ and 0·19 $g$, respectively.

Previous finite element analyses of the Long Valley Dam have been performed by Lai and Seed [3] using an equivalent linear method. In this method, the non-linear behaviour of the dam is modelled using an equivalent linear procedure to describe changes in the shear modulus and damping ratio with strain.

Griffiths and Prevost [4] performed two-dimensional and three-dimensional finite element analyses using a multi-surface kinematic model [5] to describe the stress–strain behaviour of the soil and obtained very good agreement between the measured and computed up/downstream horizontal response, however, poor agreement was obtained in the vertical direction and was thought to be due in part to the 4-noded quadrilateral finite element discretization. Due to the stiffening effect of the narrow canyon, the three-dimensional analysis gave marginally better results, but finite element frequencies tended to be over estimated due to degradation of the stiffness during shaking. It was later shown by Griffiths and Prevost [6] that small changes in the form of the stress–strain response of the soil using the multi-surface kinematic model could significantly influence the computed peak crest acceleration, demonstrating the sensitivity of the analysis to the material parameters.

In this paper, a simple elastic–perfectly plastic soil model is used to describe the stress–strain response of the soil and viscous damping is used to account for the lack of hysteretic damping. The effect of the damping ratio and the initial stress distribution are considered and the results of the analyses are compared to the measured response of the dam and to results presented by Griffiths and Prevost [4].

## A FINITE ELEMENT DISCRETIZATION AND SOIL PROPERTIES

Figure 2 shows the finite element mesh used in the analysis, representing the widest section of the dam in the up/downstream direction; the response of the dam in the transverse direction is not considered (plane-strain). The mesh consists of 448 nodes, 131 eight-node quadrilateral elements and 778 degrees of freedom in the $x$ and $y$ directions. Also shown in Fig. 2 are the location of the nine material properties groups used to model the spatial variation in the stiffness, shown in Table 1.

The material data represent typical values from previous analyses [4, 7] in which similar core and shell material properties were used and a $K_0$ initial stress

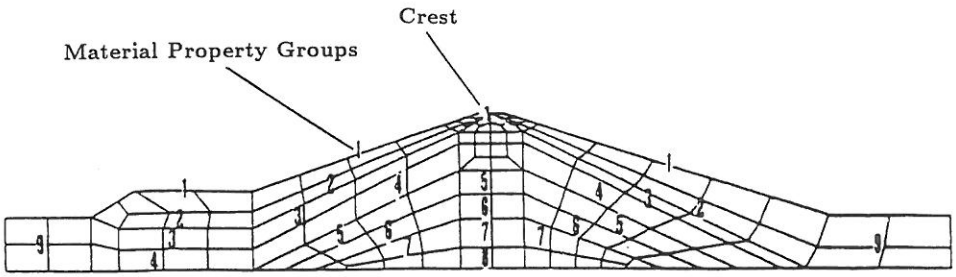


**Fig. 2.** Finite element discretization.

**TABLE 1**
Material properties for Long Valley Dam analysis

| *Group* | $E_o$ *kPa* | $v_o$ | $\phi'$ | $c'$*kPa* |
|---|---|---|---|---|
| 1 | 1·6E5 | 0·3 | 40 | 0 |
| 2 | 2·1E5 | 0·3 | 40 | 0 |
| 3 | 4·0E5 | 0·45 | 39 | 45 |
| 4 | 5·0E5 | 0·45 | 39 | 45 |
| 5 | 5·5E5 | 0·45 | 39 | 45 |
| 6 | 5·9E5 | 0·45 | 39 | 45 |
| 7 | 6·2E5 | 0·45 | 39 | 45 |
| 8 | 6·5E5 | 0·45 | 39 | 45 |
| 9 | 4·9E6 | 0·3 | — | — |

condition was assumed. In these analyses a Poisson's ratio of 0·45 was assigned for the core, since its permeability was not as low as would be expected in a dam with a narrow clay core. The rock-fill shell was considered free-draining so a Poisson's ratio of 0·3 was assigned. Although not considered in this paper, a 2 or 3 phase analysis would be necessary if accurate modelling of the water flow in the rock-fill shell were required. The influence of the bulk modulus was not considered important on the fundamental motion in the up/downstream direction.

The initial stress distribution could be specified by several different methods. In the first instance a $K_0$ condition could be assumed with $K_0 = 1$ for the core and $K_0 \approx 1 - \sin \phi$ for the shell [4, 7], in the second a "gravity turn-on" procedure [8] could be assumed. In this method, initial stresses are set by accumulating elemental weights into a global load vector, which is subsequently applied in one increment before the dynamic analysis. A third method could be adopted in which the initial stresses are calculated by "building the dam in layers," however, the earthquake being modelled was not the first seismic event that the dam experienced and so the actual initial stress distribution would not be known. In the present analysis, the first

two methods are used on the grounds of simplicity and for comparison to the kinematic model [4, 5], in which a $K_0$ initial stress state was used.

The dam is built over solid bedrock and so the boundary conditions for the finite element mesh simplify to full restraints at the base and sides. The input motions were taken from the measured bedrock accelerations (accelerographs 11 and 13 in Fig. 1) and the computed response of the dam at each time step ($\Delta t$ = 0·02 s) can be compared directly to the measured response at accelerographs 20 and 21 (crest).

## NUMERICAL ALGORITHM AND NATURAL FREQUENCY ANALYSIS

An implicit Newmark $\gamma$, $\beta$ method was used with $\gamma = 0{\cdot}5$ and $\beta = 0{\cdot}25$, representing no numerical damping. All damping generated in the analysis would therefore be due to either viscous damping or by plastic deformation when the Gauss point stress state reaches the failure surface. By increasing these parameters (e.g. $\gamma = 0{\cdot}55$, $\beta = (\gamma + 1/2)^2/4 = 0{\cdot}28$) numerical damping at high frequencies could be generated. A consistent mass discretization with $\rho = 2000$ kg/m$^3$ was assumed for all the material property groups. The horizontal and vertical input acceleration time histories were applied as inertia forces and the equation of motion solved at every time step. The non-linear algorithm is of the "initial stress" [8, 9] type and convergence was said to have occurred when the change in the displacements, non-dimensionalized with respect to the largest absolute value from one iteration to the next, was less than $1 \times 10^{-3}$.

Two-dimensional and three-dimensional natural frequency analyses of the Long Valley Dam have been performed by Griffiths and Prevost [4], Woodward and Griffiths [10] and Woodward [11]. The results of the computed two-dimensional natural frequency analysis are shown in Table 2, compared to the frequencies obtained from a spectral analysis of the measured response of the dam, and are in acceptable agreement. Three-dimensional natural frequency analyses indicate that the narrow valley sides of the dam create a stiffening effect, increasing the fundamental frequency. Woodward [11] performed parametric studies and showed how the three-dimensional natural frequency of the dam changes as the geometry of the canyon varies. This stiffening effect, however, is not considered in the present analysis.

Figure 3 shows the first four mode shapes, with the fundamental mode shape clearly in the up/downstream direction. It should be noted that higher mode shapes computed from a three-dimensional analysis are not necessarily the same as those from a two-dimensional analysis due to the effect of the transverse direction. This can account for some of the differences in the higher natural frequencies (Table 2).

**TABLE 2**
Eigenvalue analysis

| Mode | *Griffiths and Prevost [4]* *Spectral analysis (Hz)* | *2-d 4-node (Hz)* | *Present work 2-d 8 node (Hz)* |
|---|---|---|---|
| 1 | 1·85 | 1·76 | 1·79 |
| 2 | 2·15 | 2·58 | 2·63 |
| 3 | 2·45 | 3·00 | 3·07 |
| 4 | 2·65 | — | 3·35 |

Figure 4a shows the three Rayleigh damping curves considered. The frequency $f_1$ is set at the fundamental frequency of the dam, i.e. $f_1 = 1{\cdot}79$ Hz, with trial values of $f_2 = 2{\cdot}6$, 4·0 and 7·0 Hz, respectively, for a target damping ratio of $\xi_t = 3\%$. The actual damping ratio $\xi$ can then be found through equation (1),

$$\xi = \frac{1}{2}\left(\frac{\alpha}{\omega} + \beta\omega\right) \tag{1}$$

where $\alpha$ and $\beta$ are given by,

$$\alpha = 2\omega_1\omega_2\xi_t\left[\frac{\omega_1 - \omega_2}{\omega_1^2 - \omega_2^2}\right] \tag{2}$$

$$\beta = 2\xi_t\left[\frac{\omega_1 - \omega_2}{\omega_1^2 - \omega_2^2}\right] \tag{3}$$

$\omega_1$ and $\omega_2$ are the two frequencies defining the damping curve in rads/s. Since the response in the up/downstream direction is more important the curve corresponding to $f_1 = 1{\cdot}79$ Hz and $f_2 = 4{\cdot}0$ Hz is considered more appropriate as the damping is reasonably constant over the range in which the fundamental frequency occurs and is shown in Fig. 4b for damping ratios of $\xi = 3$, 6, 9, 12 and 15%. Further parametric studies could be performed to assess the effect of the less suitable damping curves on the peak response of the dam. It should be noted that at larger target damping ratios $\xi_t$, the damping curve tends to produce lower values of $\xi_t$ between $f_1$ and $f_2$.

The Rayleigh damping matrix $[C]$ can then be calculated in the finite element program as a linear combination of the mass $[M]$ and stiffness $[K]$ matrices through the following expression,

$$[C] = \alpha\,[M] + \beta\,[K] \tag{4}$$

As with previous analyses, damping effects of the upstream impounded water were not considered in the finite element analysis.

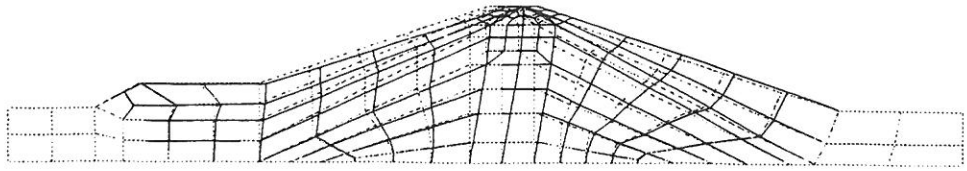

(a)

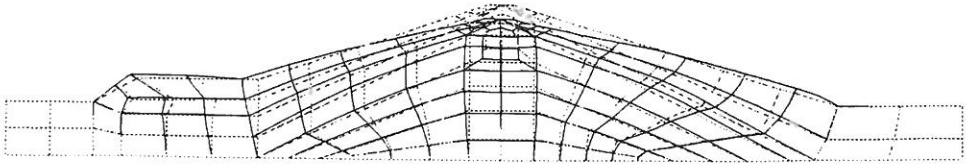

(b)

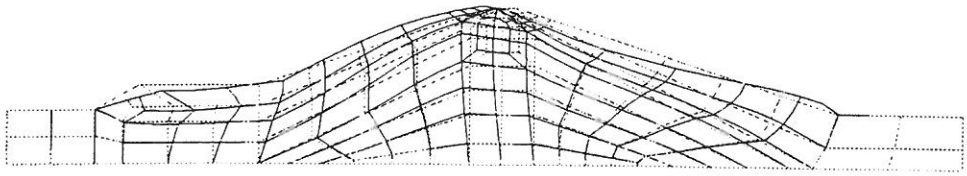

(c)

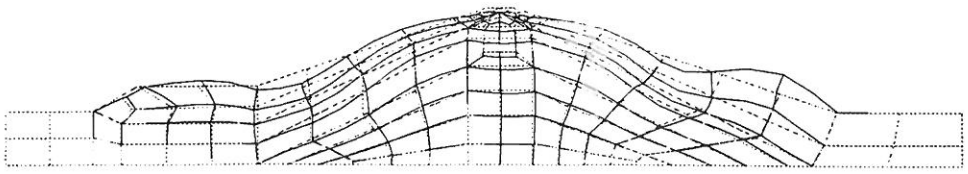

(d)

**Fig. 3.** First four mode shapes.

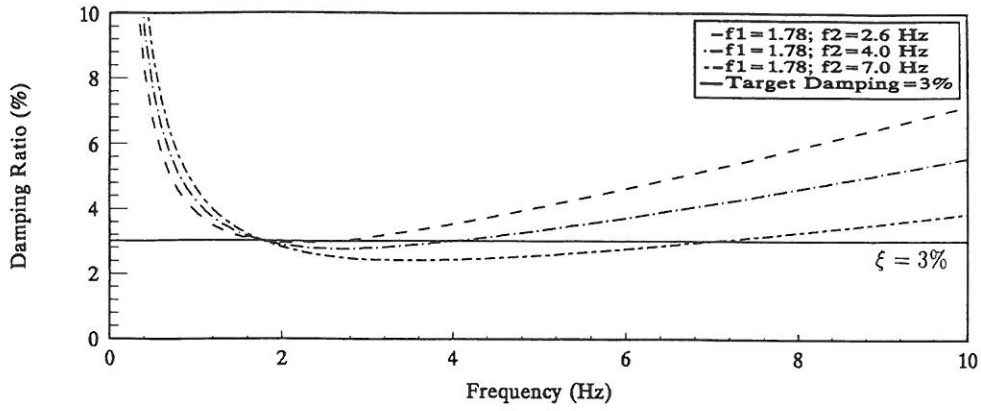


(a)

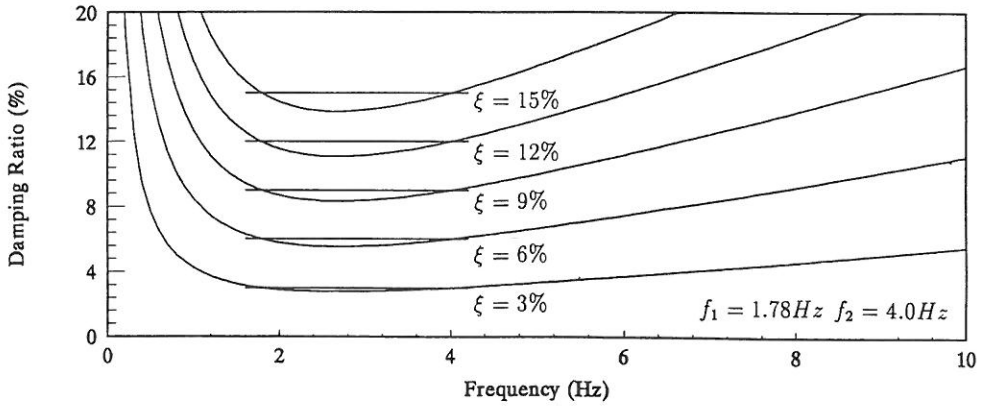


(b)

**Fig. 4.** Rayleigh damping curve. (a) Selection of damping curve at $\xi = 3\%$; (b) target damping of $\xi = 3$, 6, 9, 12 and 15%.

## INPUT MOTION

### Horizontal direction

Figure 5 shows the measured up/downstream horizontal bedrock acceleration time history (accelerograph 11 in Fig. 1) and Fourier amplitude spectrum (FAS). The total duration time of the input motion is 12 s with a peak

horizontal acceleration of –0·179 $g$ occurring ≈ 4·9 s after the start of the trace. The Fourier amplitude spectrum shows the main frequency content of the horizontal input motion in the 0·6–3·2 Hz range, with the peak energy content occurring in the 1·6–2·0 Hz range. From Table 2, the fundamental frequency of the dam also occurs within this frequency range, indicating that at low values of the viscous damping ratio $\xi$ an amplified response will be expected. This is due to hysteretic damping only being developed when the stress-state of a particular Gauss point touches the Mohr–Coulomb failure surface.

### Vertical direction

Figure 6 shows the measured vertical bedrock acceleration time history (accelerograph 13 in Fig. 1) and Fourier amplitude spectrum. The peak acceleration of 0·084 $g$ is lower than in the horizontal direction and occurs after a time interval of ≈ 5·5 s, although several peak accelerations close to this value are present during the 12 s. The Fourier amplitude spectrum shows a broader range of frequencies present, with no particular dominating frequency.

The accelerations were measured directly from the bedrock and so could be applied directly in the finite element analysis.

## TIME DOMAIN ANALYSIS

The results of the time domain analysis are summarized in Figs 7 and 8 for the two different initial stress conditions. The computed peak horizontal and vertical crest accelerations are plotted as a function of the Rayleigh damping ratio (i.e. the target damping ratio) and compared to the measured peak acceleration and to the results presented by Griffiths and Prevost [4] using the multi-surface kinematic model. For the horizontal direction damping ratios of $\xi > 9\%$ are required to reduce the computed peak acceleration close to the real measured peak, and are a direct result of the energy of the input motion peaking close to the two-dimensional natural frequency of the dam amplifying the horizontal response. At low damping ratios very little damping exists until the Mohr–Coulomb failure surface is reached, where energy is subsequently lost though plastic deformation. This is especially the case in materials 3–8 which have strong cohesive and frictional properties. In the vertical direction damping ratios greater than 4% create an excessively damped response; the real coefficient of damping of the dam, based on the induced dynamic strain for this particular earthquake, was thought not to exceed 6%.

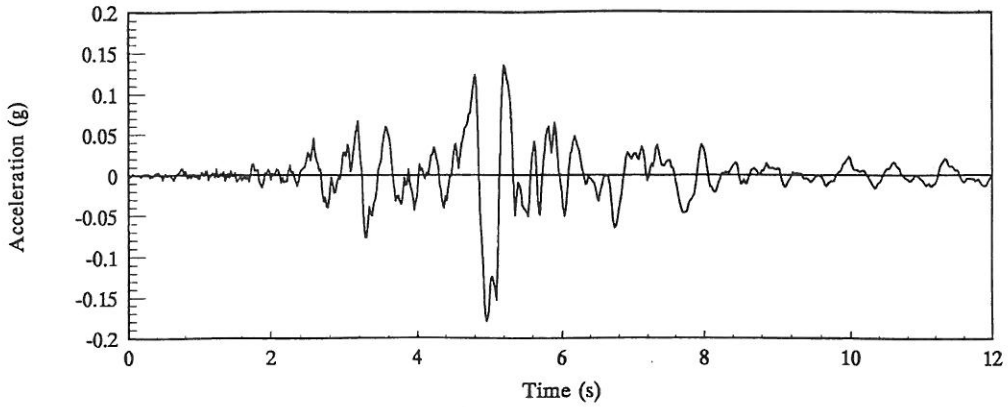


(a)

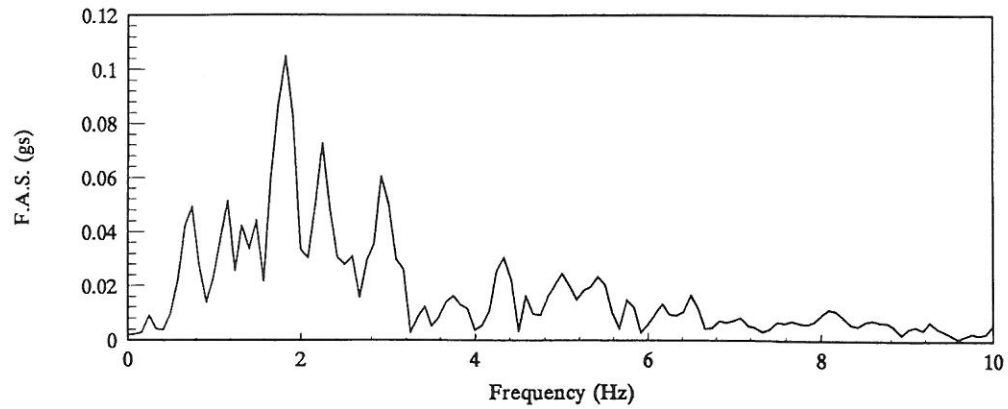


(b)

**Fig. 5.** Up/downstream base motion. (a) Acceleration; (b) Fourier amplitude spectrum.

Computing the initial stresses from a gravity turn-on procedure tends to give a slightly improved response, so a further analysis was performed in which the stress state at the end of the earthquake in the gravity turn-on case was used as the initial stress state, and the time domain analysis was performed a second time. This was to try and model a more realistic initial stress condition since this earthquake was not the first in the series of earthquakes which occurred in 1980, however, there was no significant difference

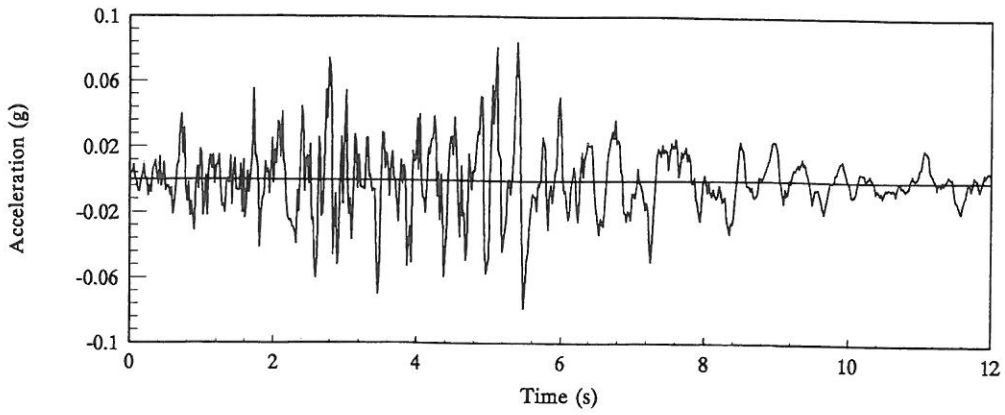


(a)

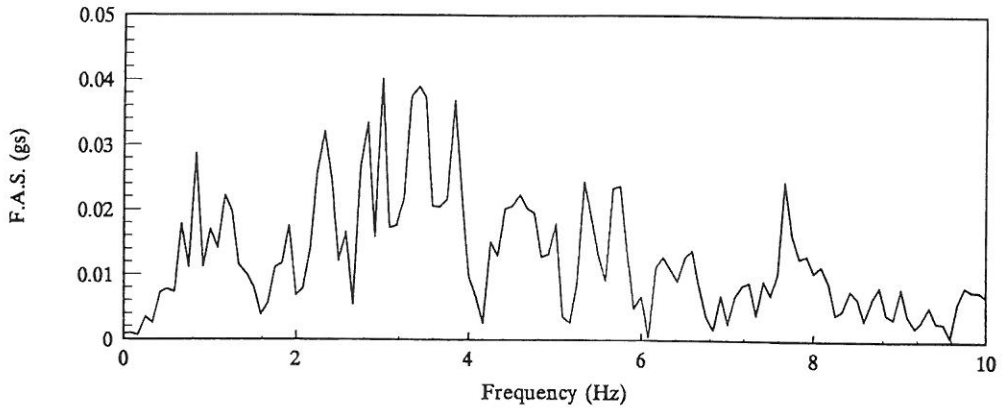


(b)

**Fig. 6.** Vertical base motion. (a) Acceleration; (b) Fourier amplitude spectrum.

in the results. If an isotropic elasto–plastic model were used in which a hardening function was applied, more change would be expected, due to alterations in the initial yield surface positions, hence influencing the level of material damping.

Figure 9 shows the computed response of the crest in the horizontal direction compared to the measured response at a damping ratio of 9%. Overall very good agreement is achieved, with the computed values giving slightly higher amplitudes. Figure 10 shows the corresponding Fourier

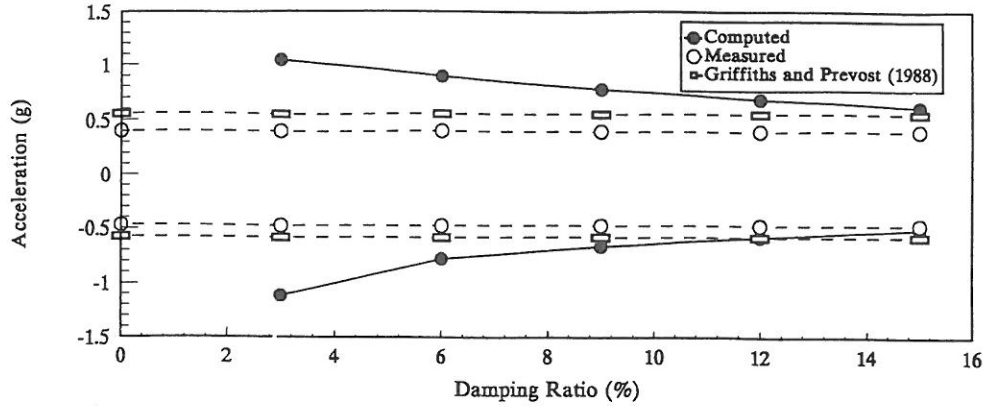


(a)

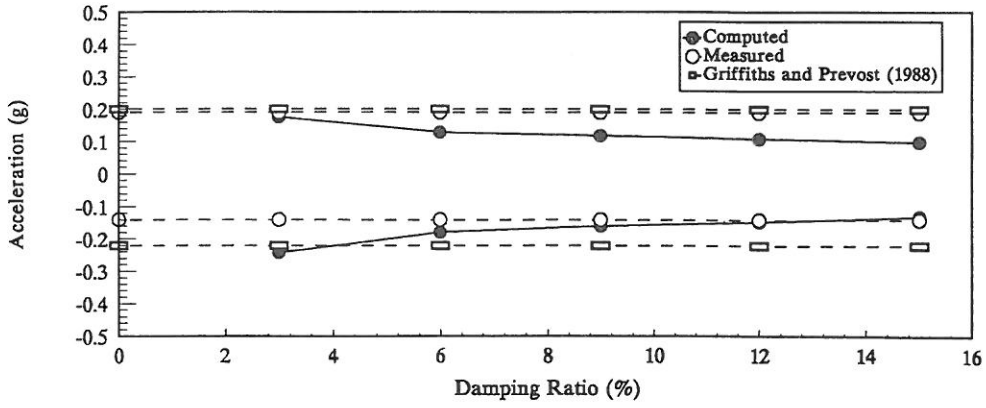


(b)

**Fig. 7.** Computed against measured peak acceleration plotted as a function of the damping ratio ($K_o$ initial stress condition). (a) Up/downstream at station 20; (b) vertical at station 21.

amplitude spectrum with the peaks in close agreement, although as with previous analyses more energy is associated with the fundamental frequency.

Figure 11 shows the computed response of the crest in the vertical direction compared with the measured response at a damping ratio of 9%. The peaks of the acceleration time history are considerably less than in the horizontal direction, however, the frequency content is higher. This creates a significant

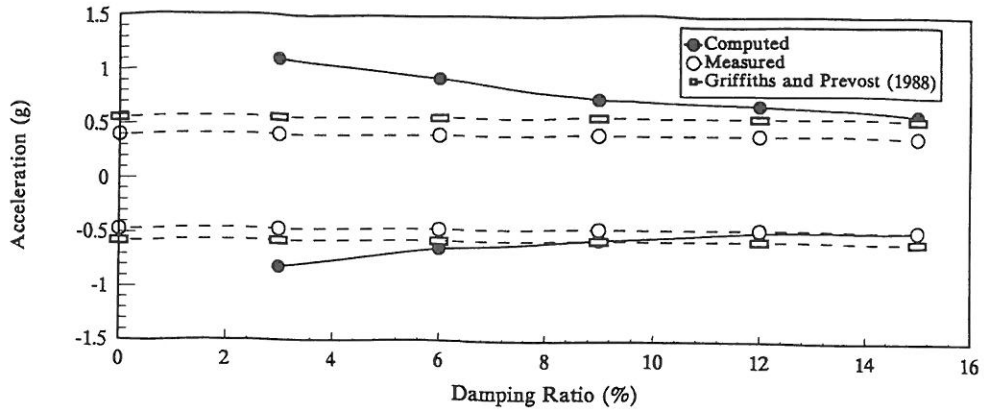


(a)

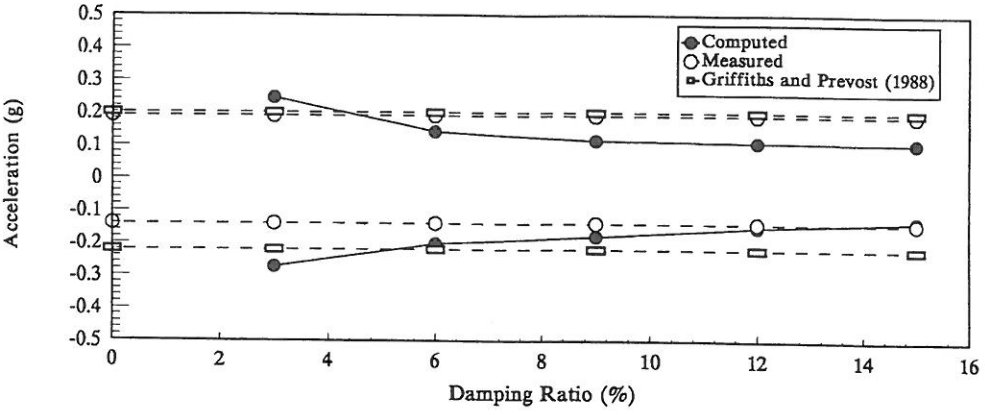


(b)

**Fig. 8.** Computed against measured peak acceleration plotted as a function of the damping ratio (gravity turn-on initial stress condition). (a) Up/downstream at station 20; (b) vertical at station 21.

amount of "noise" and makes a direct comparison difficult, although the computed response tends to be less (except at damping ratios less than 4%). Figure 12 shows the Fourier amplitude spectrum, with frequency bands mainly in the 2–4 Hz and 4·4–6 Hz range, although as with the input motion, no particular frequency is dominating the response. It is interesting to note that the multi-surface kinematic model used by Griffiths and

Prevost [4] computed energies in excess of 8 times the measured response in the 5–6 Hz frequency band. In the present analyses, at frequencies > 6 Hz, the computed energy associated with each frequency is noticeably lower than the measured, and is probably due to excessive damping caused by the Rayleigh damping curve. This highlights one of the main problems associated with applying viscous damping techniques to this type of problem. At higher frequencies there is a significant increase in the amount of damping applied. This increase in damping is dependent on the characteristics of the Rayleigh damping curve and obviously represents a serious limitation of the

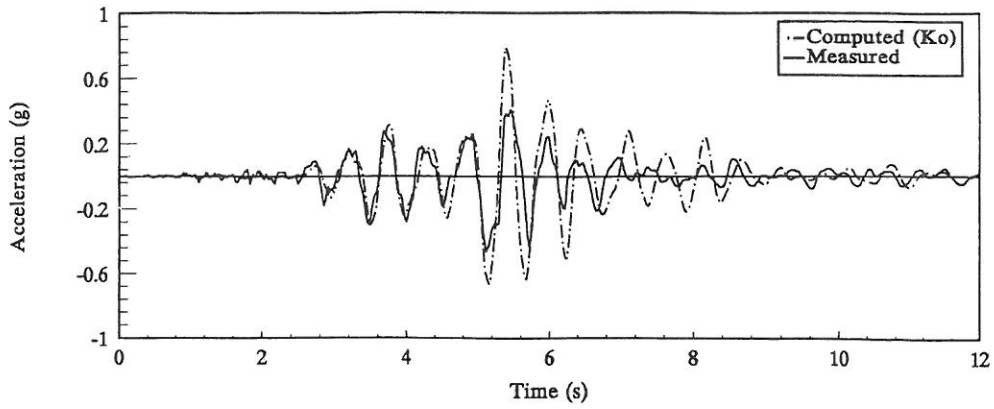


(a)

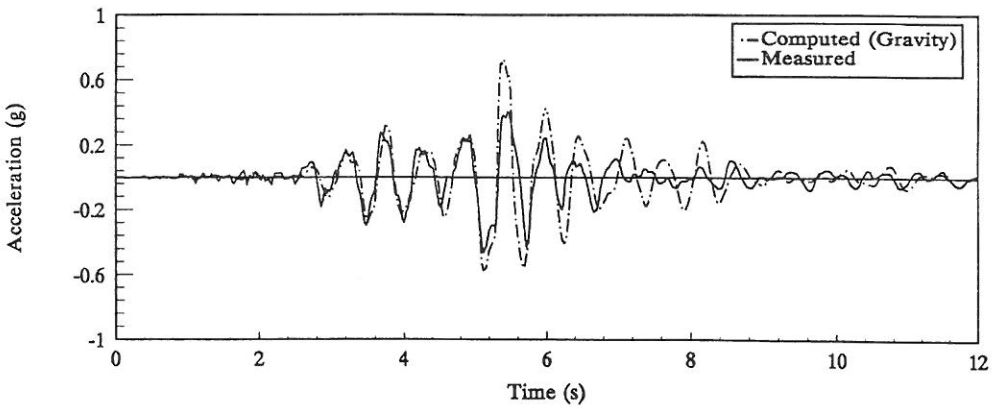


(b)

**Fig. 9.** Computed against measured motion at station 20 (up/downstream) at $\xi = 9\%$. (a) $K_o$ initial stress condition; (b) gravity turn-on initial stress condition.

method. However, the results do show that a simple constitutive model combined with viscous damping can give a good approximation to the real response of this dam in its fundamental mode, at this magnitude of earthquake excitation.

One of the main benefits of this type of analysis was that the time taken to perform each finite element simulation on a 486 PC was between 20 and 25 minutes.

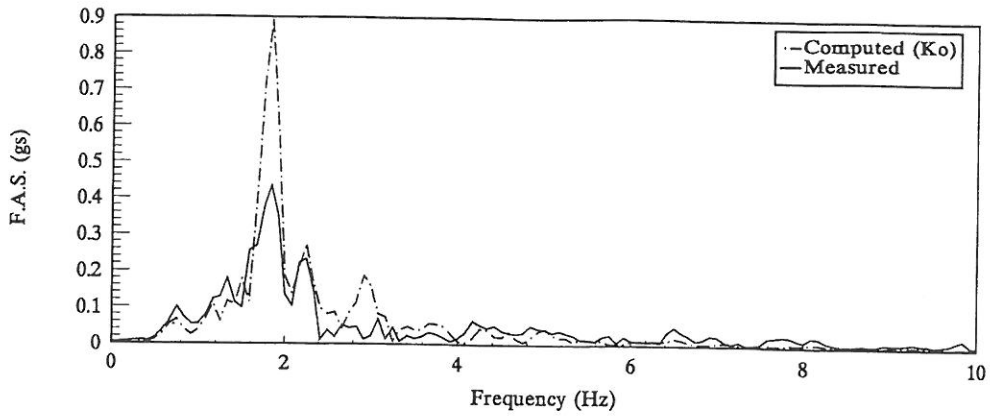


(a)

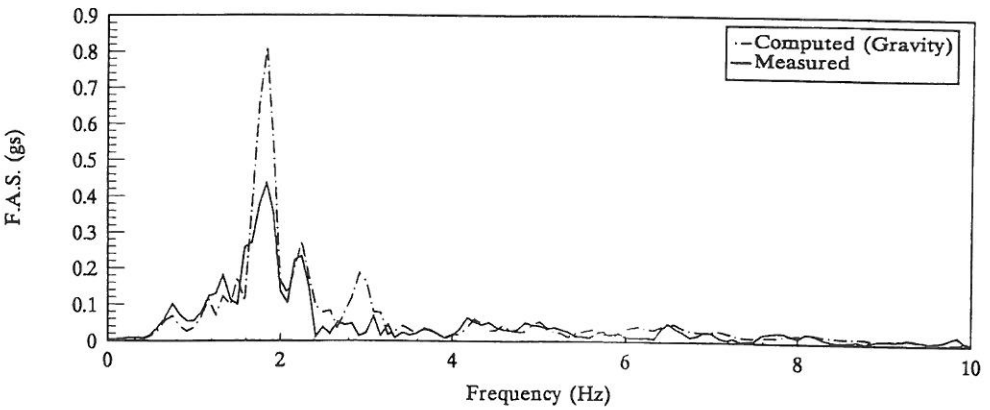


(b)

**Fig. 10.** Computed against measured Fourier amplitude spectrum at station 20 (up/downstream) at $\xi = 9\%$. (a) $K_o$ initial stress condition; (b) gravity turn-on initial stress condition.

## CONCLUSIONS

In this paper, the response of the Long Valley Dam in the Mammoth Lake area of California to seismic excitation has been computed and compared to the measured response of the dam and to the results presented by previous researchers. The results of the natural frequency analysis compare favourably to the frequencies obtained from a spectral analysis of the measured acceleration time histories. The response of the dam to the 27 May 1980 earthquake

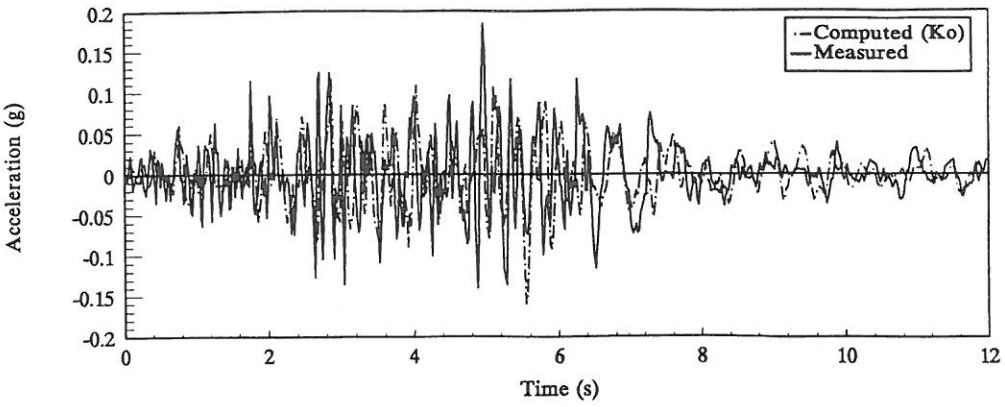


(a)

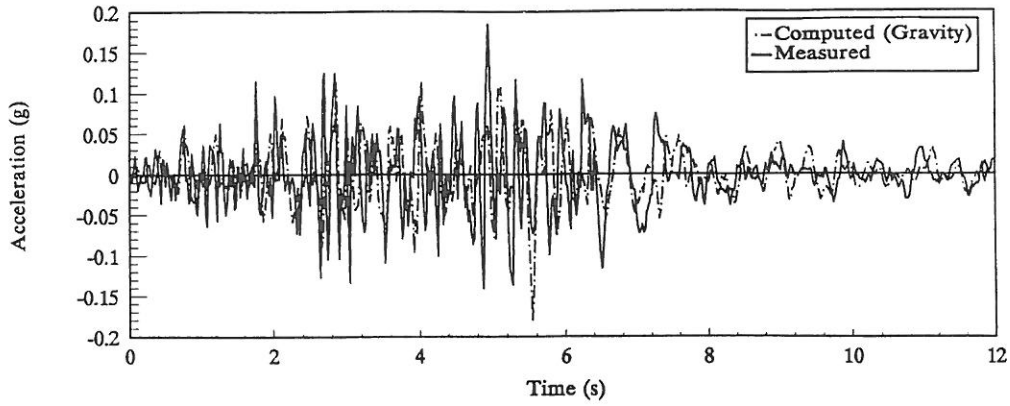


(b)

**Fig. 11.** Computed against measured motion at station 21 (vertical) at $\xi$ = 9%. (a) $K_o$ initial stress condition; (b) gravity turn-on initial stress condition.

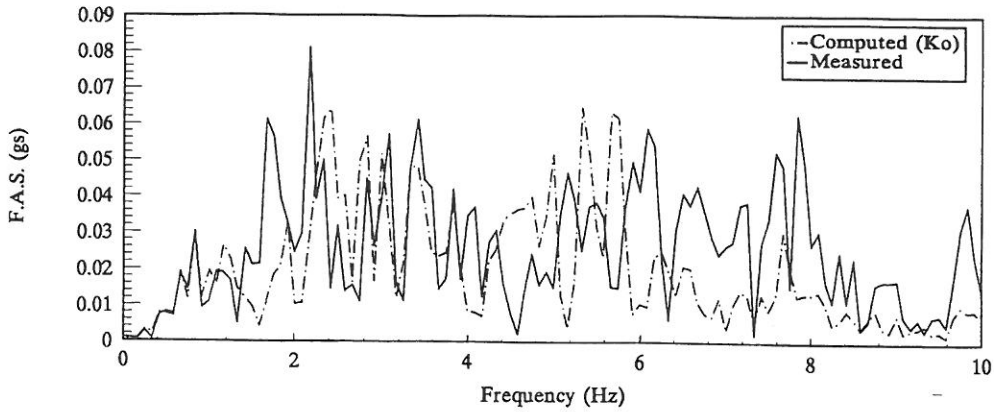


(a)

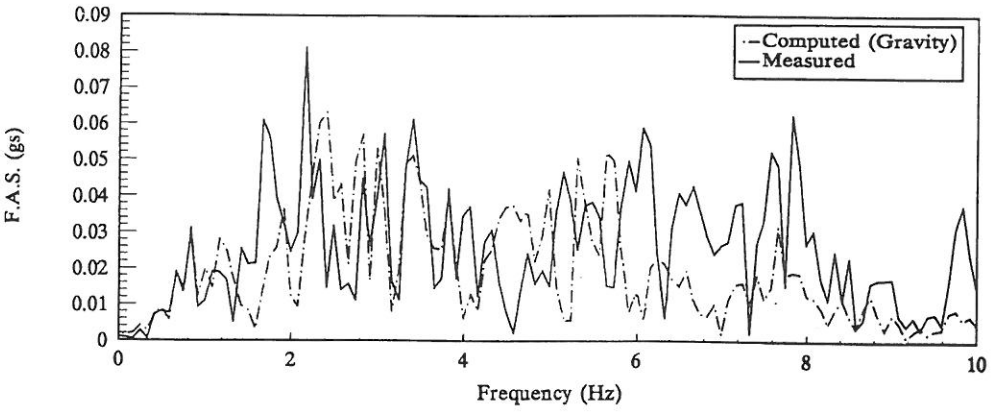


(b)

**Fig. 12.** Computed against measured Fourier amplitude spectrum at station 21 (vertical) at $\xi = 9\%$. (a) $K_o$ initial stress condition; (b) gravity turn-on initial stress condition.

has been computed using a simple elastic–perfectly plastic soil model combined with Rayleigh damping (i.e. viscous damping) to model the lack of hysteretic damping and has been shown to give a good approximation to the measured response of the dam in its fundamental mode (up/downstream direction).

Two initial stress conditions were considered; in the first a $K_o$ condition was used and in the second a gravity turn-on procedure. In both cases a Rayleigh

damping ratio of $\xi > 9\%$ was required to reduce the peak crest up/downstream acceleration close to the measured peak horizontal acceleration. The real damping coefficient of the dam during this particular earthquake was thought not to exceed 6%. This extra damping is thought to be a direct consequence of the horizontal frequency content of the input motion peaking close to the two-dimensional natural frequency of the dam, resulting in dynamic amplification in the horizontal direction. This is exacerbated because material damping is only present when the Gauss point stress state reaches the failure surface. Initial stresses computed from the gravity turn-on procedure tended to give slightly better results than those of the $K_o$ initial stress condition, and were thought to be due to the initial stress state lying closer to the failure surface.

The extra damping required in the horizontal direction tended to excessively damp the computed vertical response, although a significant proportion of the vertical frequency range was captured. At frequencies greater than 6 Hz the computed energy was lower than the measured and was due to the Rayleigh damping curve damping out the higher frequencies. This shows one of the main limitations of using viscous damping techniques in this type of problem, i.e. when the main frequency content in one direction differs significantly from that of the other. Variable damping techniques [12] could be used to specify the viscous damping coefficient based on the shear strain level in each element.

The elastic–perfectly plastic model is currently being implemented into a three-dimensional finite element program in which the stiffening effects of the valley sides can be modelled and coupling effects between the three input motions studied.

The finite element analyses have shown that simple constitutive models combined with Rayleigh damping can be used to estimate the response of the Long Valley Dam to moderately strong earthquake excitation. During the actual earthquake the dam did not suffer any serious damage, although water was observed to appear from the loosely compacted fill just beyond the toe [13]. If the build-up of excess pore water pressure becomes significant and the simulation of liquefaction (i.e. zero effective isotropic stress) becomes paramount, then the use of simple constitutive models obviously becomes very limited and more sophisticated soil models are required. One such model is the multi-surface kinematic elasto–plastic soil model ALTERNAT [14, 15] which is currently being implemented into a general coupled finite element program by the first author.

## ACKNOWLEDGEMENTS

This research was supported by SERC and W. S. Atkins North-West in the form of a CASE studentship (ref. no. 90590212) to the first author.

## REFERENCES


1. Hoye, W. W., Hegenbart, J. L. & Matsuda, S., Long Valley Dam stability evaluations. Report No AX 203-24, City of Los Angeles Dept. of Water and Power, 1982.
2. Turpen, C. D., Strong motion records from the Mammoth Lake earthquakes of May 1980 Preliminary, Report 27, California Division of Mines & Geology, Sacramento, 1980.
3. Lai, S. S. & Seed, H. B., Dynamic response of Long Valley Dam in the Mammoth Lake earthquake series of 25–27 May 1980. Report No. UCB/EERC-85/12, Earthquake Engineering Research Center, 1985.
4. Griffiths, D. V. & Prevost, J.-H., Two and three-dimensional dynamic finite element analyses of the Long Valley Dam. *Geotechnique* **38** (3) (1988) 367–388.
5. Prevost, J.-H., DYNAFLOW: a non-linear transient finite element program. Report 81-SM-1, Civil Engineering Department, Princeton University, 1981 and 1987.
6. Griffiths, D. V. & Prevost, J.-H., Hysteretic damping in the seismic analysis of an earth dam. *Fourth International Conference on Soil Dynamics and Earthquake Engineering*, Mexico City, 155–166. Computational Mechanics, 1989.
7. Prevost, J.-H., Abdel-Ghaffar, A. M. & Lacy, S. J., Non-linear dynamic analysis of an earth dam. *Journal of the Geotechnical Engineering Division, ASCE* **111** (1985) 882–897.
8. Smith, I. M. & Griffiths, D. V., *Programming the finite element method.* John Wiley & Sons, U.K., 1988.
9. Zienkiewicz, O. C., Valliappan, S. & King, I. P., Elasto–plastic solutions of engineering problems, 'initial-stress' finite element approach. *International Journal for Numerical Methods in Engineering* **1** (1969) 75–100.
10. Woodward, P. K. & Griffiths D. V. Three-dimensional finite element analyses of the natural frequencies of non-homogeneous earth dams. *Fifth International Conference on Soil Dynamics and Earthquake Engineering*, Karlsruhe 377–388. Computational Mechanics, 1991.
11. Woodward, P. K., Earthquake engineering and advanced constitutive modelling in geomechanics by finite elements. PhD Thesis, University of Manchester, Manchester, U.K., 1993.
12. Idriss, I. M., Seed, H. B. & Seriff, N. Seismic response by variable damping finite elements. *Journal of the Geotechnical Engineering Division, ASCE* **100** (1974) 1–13.
13. Seed, H. B., Lessons from the performance of earth dams during earthquakes. *Design of Dams to Resist Earthquakes.* ICE, London, 251–258 1980.
14. Molenkamp, F., Kinematic model for alternating loading ALTERNAT. LGM Report CO-218598 Delft Geotechnics (1982).
15. Molenkamp, F., Reformulation of ALTERNAT model to minimise numerical drift due to cyclic loading. University of Manchester internal report 1990.